NANO LETTERS

Letter

Confocal Raman Microscopy across the Metal#Insulator Transition of Single Vanadium Dioxide Nanoparticles

Eugenii U. Donev, Rene Lopez, Leonard C. Feldman, and Richard F. Haglund Jr.

Nano Lett., **2009**, 9 (2), 702-706• DOI: 10.1021/nl8031839 • Publication Date (Web): 28 January 2009

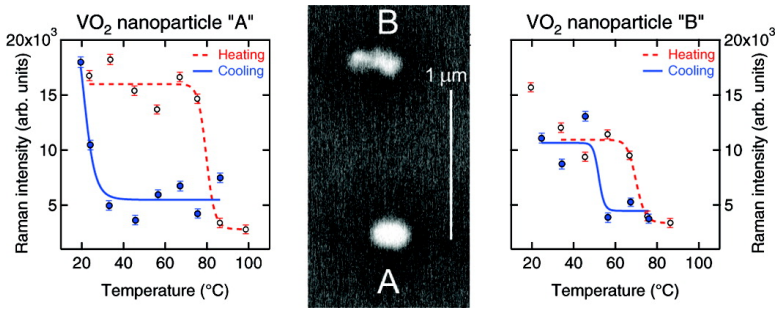

More About This Article

Additional resources and features associated with this article are available within the HTML version:

- Supporting Information
- Access to high resolution figures
- Links to articles and content related to this article
- Copyright permission to reproduce figures and/or text from this article

View the Full Text HTML

Nano Letters is published by the American Chemical Society. 1155 Sixteenth Street N.W., Washington, DC 20036

NANO LETTERS

2009
Vol. 9, No. 2
702-706

Confocal Raman Microscopy across the Metal−Insulator Transition of Single Vanadium Dioxide Nanoparticles

Eugenii U. Donev,*,† Rene Lopez,‡ Leonard C. Feldman,†,§ and Richard F. Haglund, Jr.†

Department of Physics and Astronomy and Vanderbilt Institute of Nanoscale Science and Engineering, Vanderbilt University, Nashville, Tennessee 37235, Department of Physics and Astronomy and Institute for Advanced Materials, Nanoscience and Technology, University of North Carolina, Chapel Hill, North Carolina 27514, and Institute for Advanced Materials, Devices and Nanotechnology, Rutgers, The State University of New Jersey, Piscataway, New Jersey 08854

Received October 21, 2008; Revised Manuscript Received January 14, 2009

ABSTRACT

We present the first Raman scattering measurements on nanoparticulate vanadium dioxide (VO_2), as well as the first observations of the temperature-induced phase transition in *individual* VO_2 nanoparticles (NPs). We compare the Raman response of two VO_2 NPs and a companion VO_2 film undergoing their monoclinic−tetragonal−monoclinic transformations and offer qualitative explanations for the large observed differences in hysteresis width. While bulk crystals and contiguous films contain numerous nucleation sites, individual NPs likely harbor only a few, which may make it possible to correlate detectable defects (e.g., grain boundaries and dislocations) with the "ease" of switching phases, as quantified by the width of the thermal hysteresis.

Vanadium dioxide, a transition-metal compound, has intrigued researchers for almost five decades since Morin[1] first discovered its temperature-driven metal−insulator transition ($T_c \approx 67$ °C). Accompanying the electronic transition is a change in crystallographic structure, from monoclinic (insulator/semiconductor) below T_c to tetragonal (metal).[2,3] The long-running debate[4−8] over the roles played by lattice distortion and electron−electron correlations has become quite vigorous of late, both theoretically[9] and experimentally.[10−14] Widespread interest in phase transitions in nanocrystalline systems,[15−20] and particularly the question of phase nucleation and growth from nanoscale events, has motivated the making and probing of nanoscale VO_2 in various forms. Reports on nano-VO_2 include studies of thin films of nanosize grains;[14,21−25] intertwined nanorods;[26,27] nanocrystalline powders;[28,29] and ensembles of implanted,[30−33] diffusively aggregated,[34] or lithographically patterned nanoparticles.[35,36]

However, all of these studies so far involve measuring the properties of ensembles of VO_2 nanostructures with a distribution of sizes, shapes, and defect populations. The study of single VO_2 NPs, on the other hand, offers a reasonable prospect for isolating the effect of at most a few nucleation sites on a finite, segregated volume of material to ascertain the critical size at which the metal−insulator transition can occur, if at all. In this paper, we present the first attempt to carry out such a program on single VO_2 NPs using confocal Raman microscopy, uniquely suited to pinpoint the hitherto elusive structural properties that nucleate the new phase inside the old. The application of this technique, in turn, opens the way to correlate statistically the size, structure, and defect modalities of individual nanoparticles with their observed effects on the VO_2 phase transition, thus revealing properties otherwise hidden in measurements of statistical ensembles.

Using confocal microscopy, we probed the Raman response as a function of temperature of two single VO_2 NPs (Figure 1) and a companion ("witness") patch of contiguous VO_2 film, all on the same silicon (Si) substrate. This technique is well-suited to interrogating structural changes in submicrometer particles because confocal scanning allows high-contrast imaging of an isolated NP, while Raman scattering identifies the lattice configuration of the

* Corresponding author, eugene.donev@uky.edu. Current address: Department of Electrical and Computer Engineering, University of Kentucky, Lexington, KY 40506.

† Department of Physics and Astronomy, and Vanderbilt Institute of Nanoscale Science and Engineering, Vanderbilt University.

‡ Department of Physics and Astronomy, and Institute for Advanced Materials, Nanoscience and Technology, University of North Carolina.

§ Institute for Advanced Materials, Devices and Nanotechnology, Rutgers, The State University of New Jersey.

10.1021/nl8031839 CCC: $40.75
Published on Web 01/28/2009

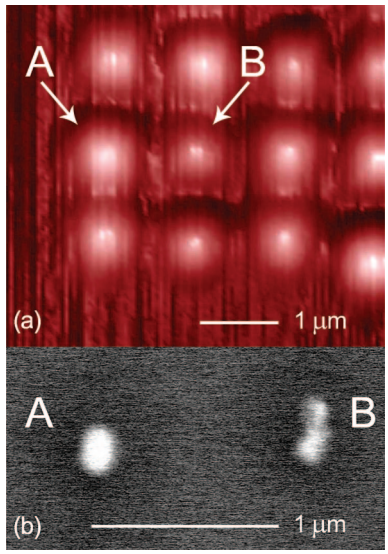

Figure 1. (a) Confocal image scan acquired at $\lambda = 633$ nm and (b) scanning electron micrograph of VO_2 nanoparticles (NPs) on Si. Note the different morphologies of NPs A and B.

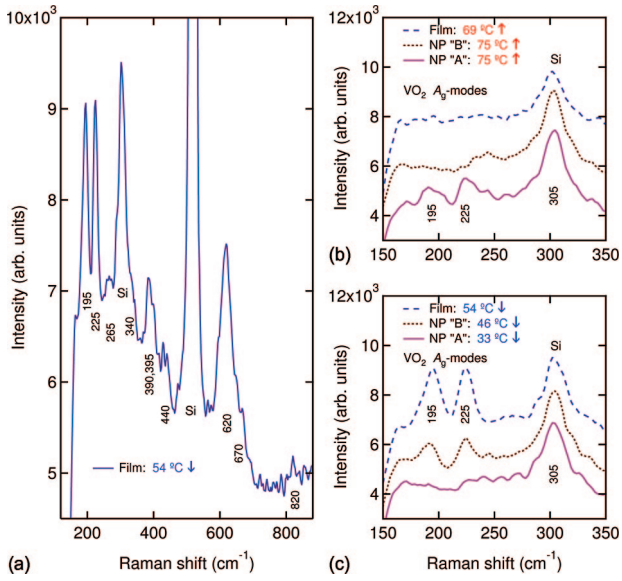

Figure 2. (a) Representative Raman spectrum of the witness film in the monoclinic (low-temperature) phase, showing several characteristic VO_2 peaks. (b) During heating (↑) toward the tetragonal (high-temperature) phase, the witness film and NP "B" complete the structural transition (A_g modes vanish) before 69 and 75 °C, respectively, while NP "A" remains at least partly untransformed at 75 °C. (c) During cooling (↓) from the high-temperature phase, NP "A" again lags thermally behind the film and NP "B" in switching back into the monoclinic phase.

NP via the spectral signature of vibrational excitations. The Raman peaks of monoclinic and tetragonal VO_2 have been reported for bulk crystals and thin films;[10,37−43] we present here the first Raman measurements on NPs of VO_2 (Figure 2). Monitoring the evolution of the Raman intensity with temperature furnished the hysteresis loop characteristic of the first-order phase transition of VO_2, which proved much wider for the NPs than for the witness film (Figure 3). To explain the three different hysteresis widths observed in this study, we invoke a model of heterogeneous nucleation of the VO_2 phase transition[44] that accounted for the size-dependence of the hysteresis in ensembles of VO_2 NPs.[30,36]

Experimental Details. We fabricated our VO_2 NPs on a Si substrate by means of: (i) focused-ion-beam lithography (FIB: 30 keV Ga^+, 1 pA current, 100 μs dwell time per NP) in a spin-coated layer of poly(methyl methacrylate) (PMMA: 50 nm thick), followed by chemical removal of the exposed areas;[35,36] (ii) pulsed-laser deposition (PLD: $\lambda = 248$ nm, V-metal target, O_2 gas at 5 mTorr) of amorphous, substoichiometric vanadium oxide ($VO_{\approx 1.7}$: 30 nm thick); (iii) chemical lift-off of the remaining PMMA and its $VO_{1.7}$ overlayer; (iv) thermal anneal (450 °C, O_2 gas at 250 mTorr) of the resulting arrays of $VO_{1.7}$ clusters to crystalline VO_2 NPs. This procedure has been demonstrated by multiple tests of stoichiometry, structure, and switching properties to produce VO_2 rather than any of the multiple competing vanadium oxides.[21] The lattice constant of the NP array was chosen large enough, about 1 μm, to ensure that individual NPs can be resolved in a confocal image scan at the laser wavelength to be used for Raman measurements. One such scan is shown in Figure 1a, with arrows pointing to the two VO_2 NPs we probed as a function of temperature. Those NPs were selected because a scanning electron micrograph (SEM) had revealed clear differences in their morphology (Figure 1b), which we suspected might lead to different phase-transition behaviors. For comparison, we also measured the Raman response of a "witness" patch of nonpatterned VO_2 film of the same deposited thickness on the same sample.

The sample was excited by continuous-wave laser light (He−Ne: $\lambda = 633$ nm, 45 mW output power), fed through a monomode fiber into a scanning near-field optical microscope (SNOM) operating in confocal-reflection mode, then focused onto the sample with a micro-objective (60×, NA = 0.80, $1/e^2$ beam spot ≈ 0.5 μm). The light scattered from the VO_2 NPs or witness film and the Si substrate was collected with the same objective in a backscattering geometry, filtered to reduce the elastic-scattering component, and sent through a multimode fiber to a spectrometer equipped with a cooled charge-coupled-device (CCD) detector. In order to minimize laser heating of the sample, the incident beam was attenuated before entering the microscope. External sample temperature was controlled (±0.5 °C) via a thermoelectric heater and a thermocouple attached to the substrate surface.

Raman measurements were performed at several fixed temperatures as follows: (1) the sample was manually positioned using micrometer drives to bring the approximate area of interest into the laser beam spot, as imaged onto a CCD camera under concurrent white-light illumination; (2) the focus was visually adjusted by vertical displacement of the microscope head; (3) the setup was then switched to confocal mode, whereby the piezoelectric sample stage would be scanned at increasing resolution and fine-adjusted laterally until the NP of interest occupied the center of a 2×2 μm^2 image scan; (4) as needed, the focus was also fine-tuned to yield a better object-to-substrate contrast; (5) finally, a 10 min Raman spectrum was collected. The sample was then

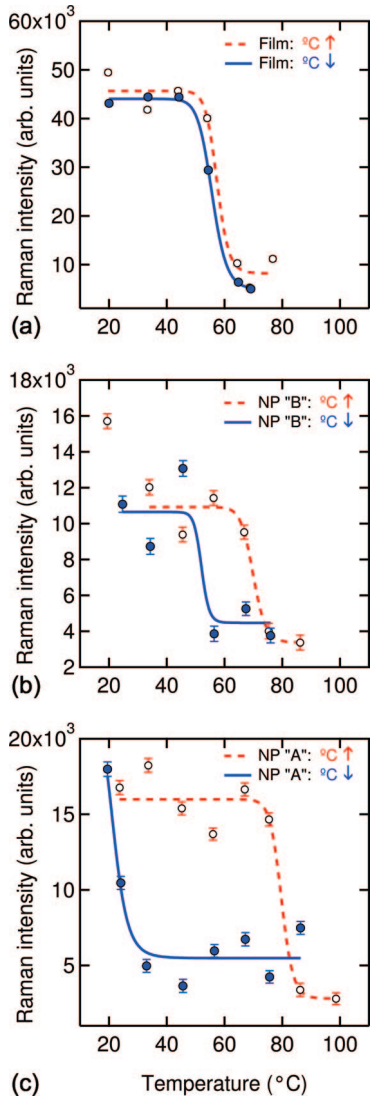

Figure 3. Thermal hystereses of the Raman intensity (165−255 cm^{-1}, less background), for (a) witness film, (b) nanoparticle "B", and (c) nanoparticle "A". Dashed and solid fit lines are for the heating (↑) and cooling (↓) half-cycles; one data point in (b) is excluded from the fit as an outlier; error bars indicate statistical uncertainty. The hysteresis width is a measure of the "ease" of switching between the low- and high-temperature states.

heated or allowed to cool, and the measurement sequence repeated at the next temperature point.

Raman Spectra. Figure 2 shows Raman spectra collected from the three VO_2-on-Si objects under investigation: the witness film patch, misshapen particle "B", and spheroidal particle "A". The complete spectrum (Figure 2a) contains several peaks that match Stokes lines assigned in the literature[39] to monoclinic VO_2, along with peaks from the Si substrate (305 and 520 cm^{-1}). The peaks near 195 and 225 cm^{-1} correspond to characteristic (A_g symmetry) vibrational modes of the monoclinic (low-temperature) structure of VO_2, which vanish upon transition into the tetragonal (high-temperature) phase.[37−40] These phonon modes play a crucial role in the structural transition of VO_2, since they are associated with the pairing and tilting motions of V−V dimers that map the monoclinic phase onto the tetragonal lattice configuration.[10] In addition, the complete disappearance of the 195 cm^{-1} peak at sufficiently high temperatures indicates that our VO_2 material does not contain measurable amounts of the V_2O_5 phase,[41] the terminal oxidation state of vanadium, which has a distinctive Raman line at 196 cm^{-1}.

Figure 2b presents snapshots of the temperature evolution of Raman intensity collected from each VO_2 object during heating of the sample toward the tetragonal phase. Only 2 °C above the bulk transition temperature of VO_2 (67 °C), the witness film no longer exhibits a monoclinic structure, as evidenced by the vanishing of the two A_g peaks (top trace) that were present at room temperature (not shown). Similarly, NP "B" has also changed structure, but not until a higher temperature of 75 °C has been reached (middle trace). Nanoparticle "A", however, has retained the monoclinic signature even at 75 °C (bottom trace)—a clear thermal delay in the onset of its monoclinic-to-tetragonal transition with respect to those of NP "B" and the witness film.

Raman spectra representative of the cooling half-cycle for each VO_2 object are shown in Figure 2c. The temperature was ramped down from a high-enough value to ensure completion of that object's forward (monoclinic-to-tetragonal) transition. By 54 °C, the witness film has already reverted to the monoclinic phase (top trace), while the A_g peaks for either NP have not yet reappeared (not shown). For NP "B", they reappear by 46 °C (middle trace), but NP "A" remains tetragonal down to at least 33 °C (bottom trace). Thus, the onset of the reverse (tetragonal-to-monoclinic) transition of NP "A" is also delayed in temperature compared to the transitions of NP "B" and the film.

We note in passing that the Si peak at 305 cm^{-1} diminishes slightly above the VO_2 phase transition due to the disappearance of an underlying VO_2 peak, usually reported around 310 cm^{-1}.[37,39−43]

Thermal Hystereses. For each of the three VO_2 objects, Figure 3 reveals the full temperature evolution of the Raman response through the thermal hysteresis that accompanies a first-order phase transition. The data points correspond to the total Raman intensity in the spectral interval containing both VO_2 peaks, summed between 165 and 255 cm^{-1} after background subtraction. The background was removed using an algorithm implementing a rolling-circle spectral filter, which distinguishes between peaks and baselines according to their radii of curvature.[45] The smooth lines through the data were obtained by least-squares fitting of an empirical sigmoidal function and used to estimate the transition midpoints for the heating and cooling branches of each hysteresis. The comparatively large scatter in Figure 3b likely stems from a variable overlap between the laser beam spot and the irregular shape of NP "B" (Figure 1b) during different measurement sequences.

The most striking features of the three hysteresis loops are their very different widths—from 2 ± 1 °C for the witness film (Figure 3a) to 18 ± 2 °C for NP "B" (Figure 3b) and 56 ± 5 °C for NP "A" (Figure 3c). In general, a first-order phase transformation requires some amount of overheating (undercooling) above (below) the equilibrium transition temperature, where the free-energy curves of the two phases intersect with a discontinuity in the first derivative. At

thermodynamic equilibrium, the system occupies one of the two (meta)stable states depending on the transformation history, i.e. whether the temperature has been increasing or decreasing. For example, martensitic structural transformations,[46] a class to which the VO_2 phase transition belongs,[47] take place at two constant temperatures when only a single interface between the two phases is involved (e.g., in single crystals). However, the transition points for a martensitic transformation vary over a range of temperatures in the case of multiple interfaces as in polycrystals.[48]

Specifically for VO_2, the sharpness, shape, width, position, and switching ratio of the thermal hysteresis have been shown to depend critically on the quality of the VO_2 material (crystallinity, stoichiometry, impurities);[21,49−51] on the grain size, distribution, and orientation;[22,23,47,52,53] as well as on NP size.[36,44] Considering the statistical characteristics of heterogeneous nucleation of martensitic transformations,[54,55] Lopez et al. have proposed an explanation of the increasingly wider hystereses (up to 50 °C) with decreasing NP sizes, as observed in near-infrared transmission through VO_2 NPs implanted into silica.[44] According to the model, a small VO_2 particle has a certain probability of switching phases that depends, for any given temperature, on the availability of "potent defects". These defects are envisioned as randomly distributed sites where the free-energy barrier is low enough for the new phase to nucleate inside the parent phase. The probability of finding at least one such nucleation site per particle, and hence the probability of transformation, is modeled phenomenologically as a function of particle volume and the temperature-dependent excess driving force.[55] A small amount of VO_2 material, such as our NP "A" or "B", would require substantial overheating and undercooling beyond the nominal transition temperature (i.e., excess driving forces) to change from the monoclinic to tetragonal phase and back, thereby exhibiting a wide thermal hysteresis (Figure 3, curves b and c).

On the other hand, our witness film switches phases with a much narrower hysteresis (Figure 3a) because the transformation of the probed region can effectively begin at any one of many possible nucleation sites distributed throughout the volume of the VO_2 film. In other words, even relatively small excursions in temperature would likely activate a few potent defects and initiate the phase transition of the entire film. An amorphous $VO_{1.7}$ film, deposited as a smooth conformal layer at room temperature, often crystallizes upon high-temperature annealing into a contiguous VO_2 film forming a network of interconnected grains with approximate sizes between 50 and 350 nm. The role of the grain boundaries, where various defects typically abound, actually competes with the pure size effect described above, to the extent that a large-grain VO_2 film may yield a wider hysteresis than a small-grain film.[21,23,53]

The above arguments help explain why the Raman hysteresis loops of our NPs are much wider than that of the witness film: The "ease" of switching depends on the presence of nucleation sites, which become more scarce as the accessible VO_2 volume shrinks. But why is NP "B" much "easier" to switch than NP "A" ($\Delta T_B = 18 \pm 2$ °C vs $\Delta T_A = 56 \pm 5$ °C) when both NPs should have the same volume, predetermined by lithography and deposition? Figure 1b offers a possible explanation. The evident differences in surface morphology may indicate that NP "A" comprises one single-crystal grain, whereas NP "B" is more "defective", i.e., possibly containing grain boundaries, dislocations, or other structural imperfections.

As in the case of the contiguous film, these features arise during the postdeposition annealing process, whereby a lithographically patterned array of amorphous $VO_{1.7}$ NPs, visually almost indistinguishable under the SEM, crystallize into an array of "individualized" VO_2 NPs. Postannealing SEM inspection usually reveals that some of the VO_2 NPs on a Si substrate are highly spheroidal or slightly elongated single units, like water droplets on a hydrophobic surface, while others resemble adjoining soap bubbles, with two or three truncated sections separated by interfacial regions. Presumably, such regions contain additional nucleation sites capable of initiating the phase transition, thus narrowing the hysteresis loops for these more "defective", compound particles. We have routinely found compound VO_2 NPs as small as 50 nm across, but also single-unit VO_2 NPs larger than 200 nm in diameter, and vice versa. Without direct measurements of the underlying crystallinity of NPs "A" and "B", we can only surmise their structural integrity based on their outward appearance (Figure 1b). Nevertheless, being able to visually differentiate the two particles exemplifies the notion of the stochastic nature of the VO_2 phase transition, namely, that VO_2 NPs of a given volume do not have a unique T_c but only a probability of switching centered at that temperature.[36]

Summary and Outlook. We have described the first observations of the phase transition in individual VO_2 NPs and the evolution of their Raman response as a function of temperature. In accord with our previous results from ensembles of VO_2 NPs,[36,44] the two single NPs studied here exhibited thermal hysteresis loops much wider than that of a companion thin film (Figure 3). In fact, NP "A" (Figure 1b) produced one of the widest VO_2 hysteresis reported to date: $\Delta T_A = 56 \pm 5$ °C. Such large thermal delays in the monoclinic−tetragonal−monoclinic transition cycles for isolated nanoscale amounts of VO_2 material have been attributed to the diminished availability of nucleation sites, active at a given temperature, as the volume of material decreases.[44] Various randomly occurring defects (vacancies, dislocations, untransformed embryonic regions, etc) can become potent sites for heterogeneous nucleation, so that even NPs of identical volumes may transform with different "ease", i.e., different hysteresis widths (Figure 3b vs Figure 3c).

The single-particle measurements reported here afford a direct way to obtain statistical information on the distribution of potent nucleation sites, namely, by spatio-thermal confocal mapping of the Raman (or other optical) response of arrays of widely spaced VO_2 nanocrystals of a given size. Armed with many single-NP hystereses and the corresponding particle morphologies, or even electron-diffraction pat-

terns,[14,56] one can gain valuable insight into the microscopic origins of the phase transition of vanadium dioxide at special lattice sites.

Acknowledgment. We thank A. B. Hmelo for help with FIB lithography and J. Rozen for help with late-night data acquisition. This work was supported by the National Science Foundation Nanoscience Interdisciplinary Research Team Grant (DMR-0210785) and by the United States Department of Energy, Office of Science (DE-RG02-01ER45916).

References

(1) Morin, F. J. *Phys. Rev. Lett.* **1959**, *3*, 34–36.
(2) Goodenough, J. B. *Am. Ceram. Soc. Bull.* **1971**, *50*, 390.
(3) Imada, M.; Fujimori, A.; Tokura, Y. *Rev. Mod. Phys.* **1998**, *70*, 1039–1263.
(4) Zylbersztejn, A.; Mott, N. F. *Phys. Rev. B* **1975**, *11*, 4383–4395.
(5) Paquet, D.; Hugon, P. L. *Phys. Rev. B* **1980**, *22*, 5284–5301.
(6) Wentzcovitch, R. M.; Schulz, W. W.; Allen, P. B. *Phys. Rev. Lett.* **1994**, *73*, 3043–3043.
(7) Rice, T. M.; Launois, H.; Pouget, J. P. *Phys. Rev. Lett.* **1994**, *73*, 3042–3042.
(8) Wentzcovitch, R. M.; Schulz, W. W.; Allen, P. B. *Phys. Rev. Lett.* **1994**, *72*, 3389–3392.
(9) Biermann, S.; Poteryaev, A.; Lichtenstein, A. I.; Georges, A. *Phys. Rev. Lett.* **2005**, *94*, 026404.
(10) Cavalleri, A.; Dekorsy, T.; Chong, H. H. W.; Kieffer, J. C.; Schoenlein, R. W. *Phys. Rev. B* **2004**, *70*, 161102.
(11) Kim, H. T.; Lee, Y. W.; Kim, B. J.; Chae, B. G.; Yun, S. J.; Kang, K. Y.; Han, K. J.; Yee, K. J.; Lim, Y. S. *Phys. Rev. Lett.* **2006**, *97*, 266401.
(12) Qazilbash, M. M.; Brehm, M.; Chae, B. G.; Ho, P. C.; Andreev, G. O.; Kim, B. J.; Yun, S. J.; Balatsky, A. V.; Maple, M. B.; Keilmann, F.; Kim, H. T.; Basov, D. N. *Science* **2007**, *318*, 1750–1753.
(13) Kübler, C.; Ehrke, H.; Huber, R.; Lopez, R.; Halabica, A.; Haglund, R. F., Jr.; Leitenstorfer, A *Phys. Rev. Lett.* **2007**, *99*, 116401.
(14) Baum, P.; Yang, D. S.; Zewail, A. H. *Science* **2007**, *318*, 788–792.
(15) Wang, C. X.; Yang, G. W. *Mater. Sci. Eng., R* **2005**, *49*, 157–202.
(16) Yamashita, I.; Kawaji, H.; Atake, T.; Kuroiwa, Y.; Sawada, A. *Phys. Rev. B* **2003**, *68*, 092104.
(17) Shirinyan, A. S.; Wautelet, M. *Nanotechnology* **2004**, *15*, 1720–1731.
(18) Goya, G. F.; Veith, M.; Rapalavicuite, R.; Shen, H.; Mathur, S. *Appl. Phys. A: Mater. Sci. Process.* **2005**, *80*, 1523–1526.
(19) Dick, K.; Dhanasekaran, T.; Zhang, Z.; Meisel, D. *J. Am. Chem. Soc.* **2002**, *124*, 2312–2317.
(20) Zaziski, D.; Prilliman, S.; Scher, E. C.; Casula, M.; Wickham, J.; Clark, S. M.; Alivisatos, A. P. *Nano Lett.* **2004**, *4*, 943–946.
(21) Suh, J. Y.; Lopez, R.; Feldman, L. C.; Haglund, R. F., Jr. *J. Appl. Phys.* **2004**, *96*, 1209–1213.
(22) Brassard, D.; Fourmaux, S.; Jean-Jacques, M.; Kieffer, J. C.; El Khakani, M. A. *Appl. Phys. Lett.* **2005**, *87*, 051910.
(23) Aliev, R. A.; Andreev, V. N.; Kapralova, V. M.; Klimov, V. A.; Sobolev, A. I.; Shadrin, E. B. *Phys. Solid State* **2006**, *48*, 929–934.
(24) Rozen, J.; Lopez, R.; Haglund, R. F., Jr.; Feldman, L. C. *Appl. Phys. Lett.* **2006**, *88*, 081902.
(25) Nagashima, K.; Yanagida, T.; Tanaka, H.; Kawai, T. *J. Appl. Phys.* **2007**, *101*, 026103.
(26) Kam, K. C.; Cheetham, A. K. *Mater. Res. Bull.* **2006**, *41*, 1015–1021.
(27) Park, J.; Oh, I. H.; Lee, E.; Lee, K. W.; Lee, C. E.; Song, K.; Kim, Y. J. *Appl. Phys. Lett.* **2007**, *91*, 153112.
(28) Guinneton, F.; Sauques, L.; Valmalette, J. C.; Cros, F.; Gavarri, J. R. *J. Phys. Chem. Solids* **2001**, *62*, 1229–1238.
(29) Xu, S. Q.; Ma, H. P.; Dai, S. X.; Jiang, Z. H. *J. Mater. Sci.* **2004**, *39*, 489–493.
(30) Lopez, R.; Boatner, L. A.; Haynes, T. E.; Haglund, R. F., Jr.; Feldman, L. C. *Appl. Phys. Lett.* **2001**, *79*, 3161–3163.
(31) Lopez, R.; Boatner, L. A.; Haynes, T. E.; Feldman, L. C.; Haglund, R. F., Jr. *J. Appl. Phys.* **2002**, *92*, 4031–4036.
(32) Lopez, R.; Haynes, T. E.; Boatner, L. A.; Feldman, L. C.; Haglund, R. F., Jr. *Opt. Lett.* **2002**, *27*, 1327–1329.
(33) Rini, M.; Cavalleri, A.; Schoenlein, R. W.; Lopez, R.; Feldman, L. C.; Haglund, R. F., Jr.; Boatner, L. A.; Haynes, T. E. *Opt. Lett.* **2005**, *30*, 558–560.
(34) Pauli, S. A.; Herger, R.; Willmott, P. R.; Donev, E. U.; Suh, J. Y.; Haglund, R. F., Jr. *J. Appl. Phys.* **2007**, *102*, 073527.
(35) Lopez, R.; Suh, J. Y.; Feldman, L. C.; Haglund, R. F., Jr. *Symp. Proc. Mater. Res. Soc.* **2004**, *820*, R1.5.
(36) Lopez, R.; Feldman, L. C.; Haglund, R. F., Jr. *Phys. Rev. Lett.* **2004**, *93*, 177403.
(37) Hyun-Tak, K.; Byung-Gyu, C.; Doo-Hyeb, Y.; Gyungock, K.; Kwang-Yong, K.; Seung-Joon, L.; Kwan, K.; Yong-Sik, L. *Appl. Phys. Lett.* **2005**, *86*, 242101.
(38) Srivastava, R.; Chase, L. L. *Phys. Rev. Lett.* **1971**, *27*, 727.
(39) Schilbe, P. *Physica B* **2002**, *316*, 600–602.
(40) Pan, M.; Liu, J.; Zhong, H. M.; Wang, S. W.; Li, Z. F.; Chen, X. H.; Lu, W. *J. Cryst. Growth* **2004**, *268*, 178–183.
(41) Petrov, G. I.; Yakovlev, V. V.; Squier, J. *Appl. Phys. Lett.* **2002**, *81*, 1023–1025.
(42) Parker, J. C. *Phys. Rev. B* **1990**, *42*, 3164.
(43) Yuan, H.-T.; Feng, K.-C.; Wang, X.-J.; Li, C.; He, C.-J.; Nie, Y.-X. *Chin. Phys.* **2004**, 82.
(44) Lopez, R.; Haynes, T. E.; Boatner, L. A.; Feldman, L. C.; Haglund, R. F., Jr *Phys. Rev. B* **2002**, *65*, 224113.
(45) Brandt, N. N.; Brovko, O. O.; Chikishev, A. Y.; Paraschuk, O. D. *Appl. Spectrosc.* **2006**, *60*, 288–293.
(46) Rao, C. N. R.; Rao, K. J. *Phase transitions in solids*; McGraw-Hill: New York, 1978.
(47) Khakhaev, I. A.; Chudnovskii, F. A.; Shadrin, E. B. *Fiz. Tverd. Tela* **1994**, *36*, 1643–1649.
(48) Ortin, J.; Planes, A.; Delaey, L. Hysteresis in Shape-Memory Materials. In *The Science of Hysteresis*; Bertotti, G., Mayergoyz, I. D., Eds.; Elsevier: London, 2005; Vol. 3, pp 467−553.
(49) Griffiths, C. H.; Eastwood, H. K. *J. Appl. Phys.* **1974**, *45*, 2201–2206.
(50) Jin, P.; Nakao, S.; Tanemura, S. *Nucl. Instrum. Methods Phys. Res., Sect. B* **1998**, *141*, 419–424.
(51) Xu, C. L.; Ma, X.; Liu, X.; Qiu, W. Y.; Su, Z. X. *Mater. Res. Bull.* **2004**, *39*, 881–886.
(52) Klimov, V. A.; Timofeeva, I. O.; Khanin, S. D.; Shadrin, E. B.; Ilinskii, A. V.; Silva-Andrade, F. *Tech. Phys.* **2002**, *47*, 1134–1139.
(53) Narayan, J.; Bhosle, V. M. *J. Appl. Phys.* **2006**, *100*, 103524.
(54) Cech, R. E.; Turnbull, D. *J. Met.* **1956**, 124–132.
(55) Chen, I. W.; Chiao, Y. H.; Tsuzaki, K. *Acta Metall.* **1985**, *33*, 1847–1859.
(56) Grinolds, M. S.; Lobastov, V. A.; Weissenrieder, J.; Zewail, A. H. *Proc. Nat. Acad. Sci. U.S.A.* **2006**, *103*, 18427–18431.

NL8031839